Supporting Information

Reprogramming the microenvironment with tumor-selective angiotensin blockers enhances cancer immunotherapy

Vikash P. Chauhan [1,2,3‡], Ivy X. Chen [1,2,3‡], Rong Tong [2,4‡], Mei Rosa Ng [1], John D. Martin [1,5], Kamila Naxerova [1], Michelle W. Wu [1], Peigen Huang [1], Yves Boucher [1], Daniel S. Kohane [4], Robert Langer [2,5*], and Rakesh K. Jain [1*]

[1] Edwin L. Steele Laboratories, Department of Radiation Oncology, Massachusetts General Hospital and Harvard Medical School, Boston, Massachusetts, USA.

[2] Koch Institute for Integrative Cancer Research, Massachusetts Institute of Technology, Cambridge, Massachusetts, USA.

[3] Harvard School of Engineering and Applied Sciences, Harvard University, Cambridge, Massachusetts, USA.

[4] Laboratory for Biomaterials and Drug Delivery, Department of Anesthesiology, Division of Critical Care Medicine, Children's Hospital Boston and Harvard Medical School, Boston, Massachusetts, USA

[5] Department of Chemical Engineering, Massachusetts Institute of Technology, Cambridge, Massachusetts, USA.

‡ these authors contributed equally to this work

** Correspondence to: rlanger@mit.edu (RL), jain@steele.mgh.harvard.edu (RKJ)*

www.pnas.org/cgi/doi/10.1073/pnas.1819889116

Materials and Methods

Instruments for *in vitro* characterization: Polymer molecular weights were determined by gel permeation chromatography on a system equipped with an isocratic pump (Model 1200, Agilent) and a Waters 2400 differential refractometer. Size-exclusion columns (Viscotek LT6000L series, 300 × 7.8 mm) were connected in series to the GPC system. THF (HPLC grade, Sigma-Aldrich) at 35 °C was used as the mobile phase. High-performace liquid chromatography (HPLC) analysis was performed on a Hewlett Packard/Agilent series 1100 (Agilent) equipped with an analytical C18 reverse phase column (Kinetex, 75 × 4.6 mm, 2.6 μ, Phenomenex, Torrance, CA) and an Agilent G1315A diode array detector. The UV wavelength for ARB analysis was set at 250 nm. NMR studies were performed on a Varian 500 system (500 MHz). The sizes and zeta potentials of nanoparticles were determined on a ZetaPALS dynamic light-scattering (DLS) detector (15 mW laser, incident beam = 676 nm, Brookhaven Instruments) or Nano-ZS zetasizer (Malvern).

Polymer synthesis: For the synthesis of polyacetals from polyol and vinyl ether monomers, first tetrahydrofuran (THF) was distilled from sodium benzophenone and dichloromethane (DCM) was distilled from CaH_2. Anhydrous toluene and dimethylformamide (DMF) were purchased from Sigma-Aldrich. *P*-toluenesulfonic acid (*p*TSA, Sigma-Aldrich) was purified by dissolving *p*TSA monohydrate in toluene and azeotropically distilling at 100-110 ^{o}C for 4 hours under nitrogen in a Dean Stark apparatus. Vinyl ether was distilled at 50 ^{o}C for 1 hour under nitrogen in a Dean Stark apparatus, with the receiving flask cooled in an ice bath; the condensed (yield ~25%) solution was stored at -20 ^{o}C prior to use. One day prior to polymer synthesis, PEG (PEG400 and PEG1000 in a 1:1 molar ratio), polyol, and vinyl ether were dried separately by Schlenk line vacuum over 24 hours. For synthesis of 1-2 g polyacetal, PEG (1 mL PEG400, 1 equivalent; 2.5 g PEG1000, 1 equivalent), *p*TSA (5 mg, 0.01 equivalents), and toluene (15 mL) were added into a round-bottom flask equipped with a stirrer and azeotropically distilled at 100-110 ^{o}C for 3-4 hours under nitrogen in a Dean Stark apparatus. The solution was then cooled to 50 ^{o}C, after ~12

mL toluene was distilled from the flask. Once the solution was cooled to 50 °C, dried polyol (1 equivalent, e.g. 300 mg 1,1,1-tris(hydroxymethyl)ethane (T4) in 3 mL DMF) followed by vinyl ether (2.5 equivalents, e.g. 1 mL di(ethylene glycol) divinyl ether (VE3)) were added via a syringe under nitrogen. The clear solution was stirred for 24 hours at 50 °C, and then 100 µL trimethylamine was added to stop the polymerization. The polymer was dried using a rotary evaporator for ~30 min then further dried under Schlenk line vacuum for ~1 hour. The polymer was then precipitated in cold hexane at -20 °C for at least 6 hours, and the precipitate was washed by cold methanol and ether and dried under vacuum overnight. Caution: the polymer synthesis is highly sensitive to moisture, and the synthesis procedures involve standard air-free handling techniques under nitrogen protection. The reaction is also highly sensitive to the *p*TSA ratio, with slightly higher or lower equivalents resulting in discoloration and/or poor polymerization (SI Appendix, Fig. S1C)

For the synthesis of polyacetals from polyol and acetal monomers, first *p*TSA was dissolved in ethyl acetate (500 µL) and added to benzene solution. The ethyl acetate was distilled off, and the polymerization reaction was initiated by the addition of 2,2-dimethoxypropane equimolar to the two monomers combined. Additional doses of 2,2-dimethoxypropane (500 µL) and benzene (2 mL) were subsequently added to the reaction, every hour for six hours, via a metering funnel under nitrogen, to compensate for 2,2-dimethoxypropane and benzene that had distilled off. After 24 hours, the reaction was stopped with triethylamine (100 µL). The polymer was isolated by precipitation into cold hexanes, then the precipitate was washed by cold methanol and ether and dried under vacuum.

ARB conjugation: Valsartan (1 equivalent), 4-dimethylaminopyridine (0.1 equivalent), *N*,*N*'-dicyclohexylcarbodiimide (4 equivalent), trimethylamine (4 equivalent) and T4-VE3 polymer (1 equivalent) were mixed in a 100-mL round-bottom flask equipped with stirrer and 60 mL THF. The solution was heated at 50 °C overnight under nitrogen. The polymer solution was filtered and the filtrate was dried using a rotary evaporator for ~30 min then further dried under Schlenk line

vacuum for ~1 hour. The polymer was isolated by precipitation into cold hexanes at -20 ^{o}C for at least 6 hours, then the precipitate was washed by cold methanol, which can dissolve free ARB, and further washed by cold ether. The resulting solid was then dried under vacuum overnight and stored at -20 ^{o}C.

Nanoparticle formulation: TMA-ARB polymer in dimethylformamide (DMF, 500 μL, 10 mg/mL) was carefully pipetted into water (15 mL) under rapid stirring. The resulting TMA-ARB nanoparticles were collected following ultrafiltration (7 min, 3000 rpm, Ultracel membrane with 40,000 NMWL, Millipore, Billerica, MA) and washed with water to remove the DMF. The sizes of nanoparticles were characterized by DLS.

Nile Red pH-sensitivity assay: TMA polymer in DMF (100 μL, 2 mg/mL) was mixed with Nile Red (100 μL, 20 μg/mL) and carefully pipetted into water under rapid stirring (2 mL). Each distinct nanoparticle solution (50 μL) was added into pH 7.4 or 6.7 buffer (150 μL) in a 96 well plate. The plate was sealed, and the initial fluorescence of Nile Red was determined by the fluorescence of the particle solution at 590 nm in a microplate reader with the excitation source set at 530 nm. The plate was then incubated at 37 ^{o}C for 6 hours. The ratio of the fluorescence intensity change between pH 6.7 and 7.4 was used to calculate the pH sensitivity of the nanoparticle.

ARB release kinetics: To determine the release kinetics of the TMA-ARB, suspensions of the particles in PBS were placed into Slide-A-Lyzer dialysis tubes (300 μL each tube) with a molecular weight cutoff at 3500 Da (Pierce, Rockford, IL). These microtubes were individually dialyzed in 2 L of PBS buffer (1X, pH 7.4) or phosphate buffer (pH=6.7, prepared by NaH_2PO_4 and Na_2HPO_4) at 37 ^{o}C. The buffer was changed every 24 hours. At scheduled time points, samples were collected from the microtubes. DMF (300 μL) was added to dissolve the polymer, and the fully conjugated ARB amount was determined by treating the samples with cold 0.1mM HCl prior to

HPLC analysis. ARB content was serially subtracted from the measured starting quantity of ARB to determine release kinetics.

Tumor models: MCa-M3C cells (*Her2*+) were kindly provided by Dr. Peigen Huang, and were isolated from lung metastases of mammary adenocarcinomas in mice generating spontaneous mammary tumors (*MMTV-PyVT*) (1). Orthotopic breast tumors were generated by implanting a small piece (1 mm^3) of viable tumor tissue (from a source tumor in a separate animal) into the mammary fat pad of a 6-8 week-old female FVB (MCa-M3C model), Balb/c (4T1 model, *triple-negative*), or C57BL/6 (E0771 model, *triple-negative*) mouse. AK4.4 cells ($Kras^{G12D}$ *and* $p53^{+/-}$) were kindly provided by Dr. Nabeel Bardeesy, and were isolated from mice generating spontaneous pancreatic tumors (*Ptf1-Cre/LSL-*$Kras^{G12D}$*/*$p53^{Lox/+}$) (2). Orthotopic pancreatic tumors were similarly generated by implanting a small piece (1 mm^3) of viable tumor tissue into the pancreas of a 6-8 week-old male FVB mouse (AK4.4 model) mouse. All animal procedures were carried out following the Public Health Service Policy on Humane Care of Laboratory Animals and approved by the Institutional Animal Care and Use Committee of Massachusetts General Hospital.

Biodistribution studies: Mice bearing orthotopic MCa-M3C or AK4.4 tumors were injected with 40mg/kg valsartan, in either the 'free' unconjugated form or the TMA-ARB form, intravenously (retro-orbital injection). The mice were sacrificed 24 hours post-injection and exsanguinated through perfusion with 20 mL saline by intracardial injection. Following exsanguination, the tumors and organs were collected and flash-frozen in liquid nitrogen. ~100 mg of organ tissues were weighed and homogenized in 1 mL CelLytic tissue lysis buffer (Sigma-Aldrich) on ice for 1 min; and the homogenization was repeated for 5-10 times at 5 min intervals to allow complete decomposition of the bulk tissue. Samples were chilled in ice during the 5 min interval. Cold methanol (500 µL) was added to the homogenate, then the mixtures were vortexed for 2 minutes and then centrifuged at 12,000 rpm for 15 min (5415D Microcentrifuge, Eppendorf). To determine

the level of unconjugated (released) ARB in each tissue homogenate sample, 1 mL of the supernatant solution was filtered through an Impact protein precipitation plate (Phenomenex) then transferred into an HPLC vial and analyzed by HPLC. To assess polymer-conjugated (unreleased) ARB levels, the remaining conjugated ARB was released by addition of 250 µL of 0.1mM HCl to 750 µL of the samples in cold methanol before HPLC analysis and compared with the ARB levels without HCl addition. The data were normalized against the total injected dose per tissue mass (% I.D./g).

Histology: For breast tumors, mice bearing orthotopic MCa-M3C tumors were split into time- and size-matched (~100 mm^3) treatment groups. For pancreatic tumors, mice bearing orthotopic tumors were split into treatment groups 6 days post-implantation. The mice were then treated with 40 mg/kg valsartan in either the 'free' unconjugated form or the TMA-ARB form, or an equal volume of PBS intravenously (retro-orbital injection) each day for 6 (MCa-M3C) or 7 (AK4.4) days. The tumors were then excised, fixed in 4% formaldehyde in PBS (30 min/mm diameter of tissue), incubated in 30% sucrose in PBS overnight at 4 °C, and frozen in optimal cutting temperature compound (Tissue-Tek). Transverse tumors sections, 40 µm thick, were immunostained with antibodies to the endothelial marker CD31 (MEC13.3 antibody, BD, 1:100 dilution), and counterstained with DAPI (Vector Labs). Collagen I was detected by staining using the LF-68 antibody (1:50 dilution) provided by Dr. Larry Fisher (NIDCR). Staining for αSMA (C6198 antibody, Sigma, 1:100 dilution) was carried out in 20 µm sections. Staining for CD3-FITC (17A2 antibody, BioLegend, 1:100 dilution) was carried out in 20 µm sections.

Histological image analysis: Eight random fields (four interior, four periphery) at 20x magnification were taken from each slide using a confocal microscope (Olympus). For open versus closed lumen quantification, vessels were analyzed by eye and a vessel was counted as open if it had a clearly visible lumen throughout its length (2, 3). Images of collagen I and αSMA stained sections were analyzed based on the area fraction of positive staining through a custom MATLAB script

using built-in image processing functions. Distance mapping was carried out using a custom MATLAB script that selected CD3+ cells and calculated the distance from the centroid of each cell to its nearest αSMA+ or CD31+ cell using built-in image processing functions. Identical analysis settings and size/intensity thresholds were used for all tumors, and thresholds were determined using negative control stains utilizing only a secondary antibody.

Solid stress: Solid stress was measured using the tumor opening technique (4). When the tumors reached a size of ~1 cm in diameter, the mice were anesthetized. Subsequently, each tumor was excised, washed with Hanks' Balanced Salt Solution (HBSS) and its three dimensions were measured. Each tumor was cut along its longest axis, to a depth of 80% of its shortest dimension, using a scalpel. The tumors were allowed to relax for 10 min in HBSS to diminish any transient, poro-elastic responses. Afterwards, the opening resulting from the cut was measured at the middle of the cut at the surface of the tumor. Solid stress is proportional to the size of the opening relative to the size of the dimension perpendicular to the cut.

Mean arterial pressure: Male FVB mice of 6-8 week age were used for blood pressure measurements. Mean arterial pressure was measured using a tail cuff technique (Kent Scientific). Mice were acclimated to the device through 5 daily mock measurements in the tail cuff apparatus prior to study initiation.

RNA-sequencing: Mice bearing orthotopic MCa-M3C tumors were split into time- and size-matched (~100 mm^3) treatment groups. The mice were then treated with 40 mg/kg valsartan in the TMA-ARB form or an equal volume of PBS intravenously (retro-orbital injection) each day for 6 days. The tumors were then excised and RNA was extracted. RNA quality was assessed using a BioAnalyzer (Agilent). Poly(A) selection was carried out on these RNA samples using the NEBNext Poly(A) mRNA Magnetic Isolation Module (E7490L, NEB). Libraries for sequencing were constructed using the NEBNext Ultra Directional RNA Library Prep Kit (E7420L, NEB).

Sequencing was carried out on a HiSeq 2000 (Illumina). Using the aligner Salmon (http://salmon.readthedocs.io/en/latest/salmon.html) under default filtering settings, sequencing reads (fastqs) were aligned to, and count estimates calculated for, GenCode-annotated mouse (mm12, vM9) transcripts. The R package edgeR (5) was used to calculate differential expression between control and TMA-ARB treated tumors. The edgeR likelihood ratio (LR) was used to generate a pre-ranked gene list for Gene Set Enrichment Analysis (GSEA) (6), prepending a negative sign to the LR for genes with a negative fold change (downregulated in TMA-ARB treated tumors). GSEA was then run pre-ranked with default parameters (1000 gene set permutations, weighted enrichment statistic), using the Hallmarks and Biocarta gene set collections provided by MsigDB (http://software.broadinstitute.org/gsea/msigdb). Raw data are available from Gene Expression Omnibus, Accession number GSE98827.

Gene expression: Mice bearing orthotopic MCa-M3C or E0771 tumors were split into time- and size-matched (~100 mm^3) treatment groups. The mice were then treated with 40 mg/kg valsartan in either the 'free' unconjugated form or the TMA-ARB form, or an equal volume of PBS intravenously (retro-orbital injection) each day for 6 days. The tumors were then excised and RNA was extracted. For CD45+CD3+CD8+ cytotoxic T-lymphocyte, αSMA+ cell, PDGFRα+ CAF, and CD45+CD3-B220+ B-lymphocyte gene expression, monoclonal anti-mouse αSMA (C6198 antibody, Sigma), B220 (RA3-6B2, BioLegend), CD45 (30-F11, BioLegend), CD3 (17A2, BioLegend), CD8 (53-6.7, BioLegend), or PDGFRα (APA5, eBiosciences) antibodies were used to sort out cells following excision of the tumors and RNA was extracted. Gene expression was assessed using a qRT-PCR array for mouse cytokines, chemokines, and related genes (PAMM-150Z Qiagen) or using specific primers for *Ccl5* (F 5'-GCTGCTTTGCCTACCTCTCC-3', R 5'-TCGAGTGACAAACACGACTGC-3'), *Ccl19* (F 5'-GGGGTGCTAATGATGCGGAA-3', R 5'-CCTTAGTGTGGTGAACACAACA-3'), *Ctla4* (F 5'-TTTTGTAGCCCTGCTCACTCT-3', R 5'-CTGAAGGTTGGGTCACCTGTA-3'), *Cxcl3* (F 5'-GGCCACGGTATTCTGGAAGC-3', R 5'-

GGGCGTAACTTGAATCCGATCTA-3'), *Cxcl11* (F 5'-GGCTTCCTTATGTTCAAACAGGG-3', R 5'-GCCGTTACTCGGGTAAATTACA-3'), *Cxcl13* (F 5′-TCTCTCCAGGCCACGGTATTCT-3′, R 5′-ACCATTTGGCACGAGGATTCAC-3′), *Cxcr3* (F 5'-TACCTTGAGGTTAGTGAACGTCA-3', R 5'-CGCTCTCGTTTTCCCCATAATC-3'), *FasL* (F 5'-TCCGTGAGTTCACCAACCAAA-3', R 5'-GGGGGTTCCCTGTTAAATGGG-3'), *Gzma* (F 5'-TGCTGCCCACTGTAACGTG-3', R 5'-GGTAGGTGAAGGATAGCCACAT-3'), *Gzmb* (F 5'-TCATGCTGCTAAAGCTGAAGAG-3', R 5'-CCCGCACATATCTGATTGGTTT-3'), *H2d1* (F 5'-TACCTGAAGAACGGGAACGC-3', R 5'-ATTCAACTGCCAGGTCAGGG-3'), *Ifng* (F 5'-ATGAACGCTACACACTGCATC-3', R 5'-CCATCCTTTTGCCAGTTCCTC-3'), *Il6* (F 5'-TAGTCCTTCCTACCCCAATTTCC-3', R 5'-TTGGTCCTTAGCCACTCCTTC-3'), *Il10* (F 5'-GCTCTTACTGACTGGCATGAG-3', R 5'-CGCAGCTCTAGGAGCATGTG-3'), *Pdcd1* (F 5'-ACCCTGGTCATTCACTTGGG-3', R 5'-CATTTGCTCCCTCTGACACTG-3'), *Pdl1* (F 5'-GCTCCAAAGGACTTGTACGTG-3', R 5'-TGATCTGAAGGGCAGCATTTC-3'), and *Tnfa* (F 5'-CTTCAACTGTCCCGATGGTGA-3', R 5'-AGGCCATTATCTTTCCCTGTGA-3').

Breast tumor growth studies: Mice bearing orthotopic E0771, MCa-M3C, or 4T1 breast tumors were split into treatment groups, time-matched for time after implantation and size-matched for tumor volume at this time (82 mm^3 in E0771, 36 mm^3 in MCa-M3C, 79 mm^3 in 4T1). The mice were then treated with 40 mg/kg valsartan in the TMA-ARB form or an equal volume of PBS intravenously (retro-orbital injection) daily from days 0-7. For studies where the unconjugated polyacetal was used, the dose was 400 mg/kg (identical to the polyacetal content in the TMA-ARB dose). The immune checkpoint cocktail of anti-PD-1 (200 μg, RMP 1-14 eBioscience) and anti-CTLA-4 (100 μg, 9D9 BioXcell) was administered on days 2, 5, and 8. The primary tumors were then measured every 1-2 days, beginning on day 0, using calipers.

Flow cytometry analysis: Mice bearing orthotopic E0771 breast tumors were split into treatment groups, time-matched for time after implantation and size-matched for tumor volume at this time

(82 mm^3 in E0771). The mice were then treated with 40 mg/kg valsartan in the TMA-ARB form or an equal volume of PBS intravenously (retro-orbital injection) daily from days 0-6. The immune checkpoint cocktail of anti-PD-1 (200 µg, RMP 1-14 eBioscience) and anti-CTLA-4 (100 µg, 9D9 BioXcell) was administered on days 2 and 5. Breast tumor tissues were harvested on day 7, minced, digested, and incubated at 37 °C for 1 hour with DMEM media containing collagenase type 1A (1.5 mg/mL), hyaluronidase (1.5 mg/mL), and Dnase (2 mg/mL). The digestion mixtures were filtered through 70-µm cell strainers. Single-cell suspensions were incubated with rat anti-mouse CD16/CD32 mAb for 10 minutes at 4 °C, and then stained with fluorochrome conjugated antibodies. The stained cell suspensions were washed and resuspended in cold buffer (1% BSA, 0.1% sodium azide in PBS). Prior to flow analysis, 7-amino-actinomycin D (7AAD, eBioscience) was added to each stained tube for gating of viable cells. Flow cytometry data were obtained using an LSRII flow cytometer (Becton Dickinson) and analyzed using FACSDiva software. The double/aggregated events were gated out using forward scatter area (FSC-A) vs. forward scatter width (FSC-W) and side scatter area (SSC-A) vs. side scatter width (SSC-W). Various combinations of the following monoclonal anti-mouse antibodies were used: CD4 (RM4-5, BioLegend) , CD45 (30-F11, BioLegend), CD11b (M1/70, BioLegend), CD3 (17A2, BioLegend), CD25 (PC61, BioLegend), CD8a (53-6.7, BioLegend), FoxP3 (FJK-16s, eBioscience), Tnf-α (MP6-XT22, eBioscience), TGF-β (TW7-16B4, eBiosciences), CD279 (29F.1A12, BioLegend), B220 (RA3-6B2, BioLegend), CD274 (10F.9G2, BioLegend), CD152 (UC10-4B9, BioLegend), Granzyme B (GB11, BioLegend), IFN-γ (XMG1.2, BioLegend), CD206 (C068C2, BioLegend), MHC II (M5/114.15.2, BioLegend).

Metastatic breast cancer animal survival studies: Mice bearing orthotopic E0771, MCa-M3C, or 4T1 breast tumors were allowed to progress until the point when 100% developed spontaneous lung tumors, which occurred once the primary tumors reached a large size (1000 mm^3 in E0771 and MCa-M3C, 180 mm^3 in 4T1). The primary tumors were surgically excised at this tumor size

to leave only the metastatic disease. Mice were split into treatment groups, time-matched for the time to tumor resection after implantation and size-matched for tumor volume at resection. Treatment was initiated on day 0, which was designated as 4 (MCa-M3C) or 2 (4T1) days following primary tumor resection. The mice were then treated with 40 mg/kg valsartan in the TMA-ARB form or an equal volume of PBS intravenously (retro-orbital injection) daily from days 0-7 for immunotherapy studies or days 0-5 for chemotherapy studies. For immunotherapy studies, the immune checkpoint cocktail of anti-PD-1 (200 μg, RMP 1-14, BioXcell) and anti-CTLA-4 (100 μg, 9D9 BioXcell) was administered on days 2, 5, and 8. For chemotherapy studies, nab-paclitaxel was administered on days 2-6 at a dose of 10 mg/kg per day. The endpoint was designated as the time of death or loss of 20% of maximal body weight, whichever occurred first. Mouse lungs were collected at the endpoint and were fixed in Bouin's solution, and macrometastases were counted using a stereomicroscope.

Pancreatic tumor growth studies: Mice bearing orthotopic AK4.4 pancreatic tumors were split into treatment groups 1 day after implantation. The mice were then treated with 40 mg/kg valsartan in either the 'free' unconjugated form or the TMA-ARB form, or an equal volume of PBS intravenously (retro-orbital injection) on days 1-12. The chemotherapeutic 5FU was administered on days 5, 9, and 13 after implantation at a dose of 60 mg/kg. Tumors were extracted on day 14 for measurement using calipers.

Animal toxicity studies: Male FVB mice of 6-8 weeks age were split into treatment groups based on body weight. The mice were then treated with 40 mg/kg valsartan in either the 'free' unconjugated form or the TMA-ARB form, an equal volume of PBS, or 400 mg/kg unconjugated polyacetal (identical to the polyacetal content in the TMA-ARB dose) intravenously (retro-orbital injection) on days 1-7. For immunotherapy studies, the immune checkpoint cocktail of anti-PD-1 (200 μg, RMP 1-14, BioXcell) and anti-CTLA-4 (100 μg, 9D9 BioXcell) was administered on days 2, 5, and 8. On day 9, major organs (brain, heart, kidney, liver, lung, and spleen) were extracted,

fixed in 4% formaldehyde in PBS (30 min/mm diameter of tissue), and paraffin-embedded. The body weight and behavior of the animals were monitored daily throughout the treatment period. Histological images were assessed by a veterinary pathologist. For hematological and biochemical analysis, blood was collected by cardiac puncture. Whole blood was used to analyze complete blood counts (CBC) using an auto analyzer. Serum was separated from the whole blood and used to measure a clinical chemistry panel.

Statistical analysis: The data are presented as means with standard errors. Groups were compared using an unpaired Student's t-test, except for animal survival studies where a log-rank test was used. In pairwise comparisons within studies where multiple comparisons were made, *P* values were adjusted using Holm-Bonferroni correction.

Supporting Figures

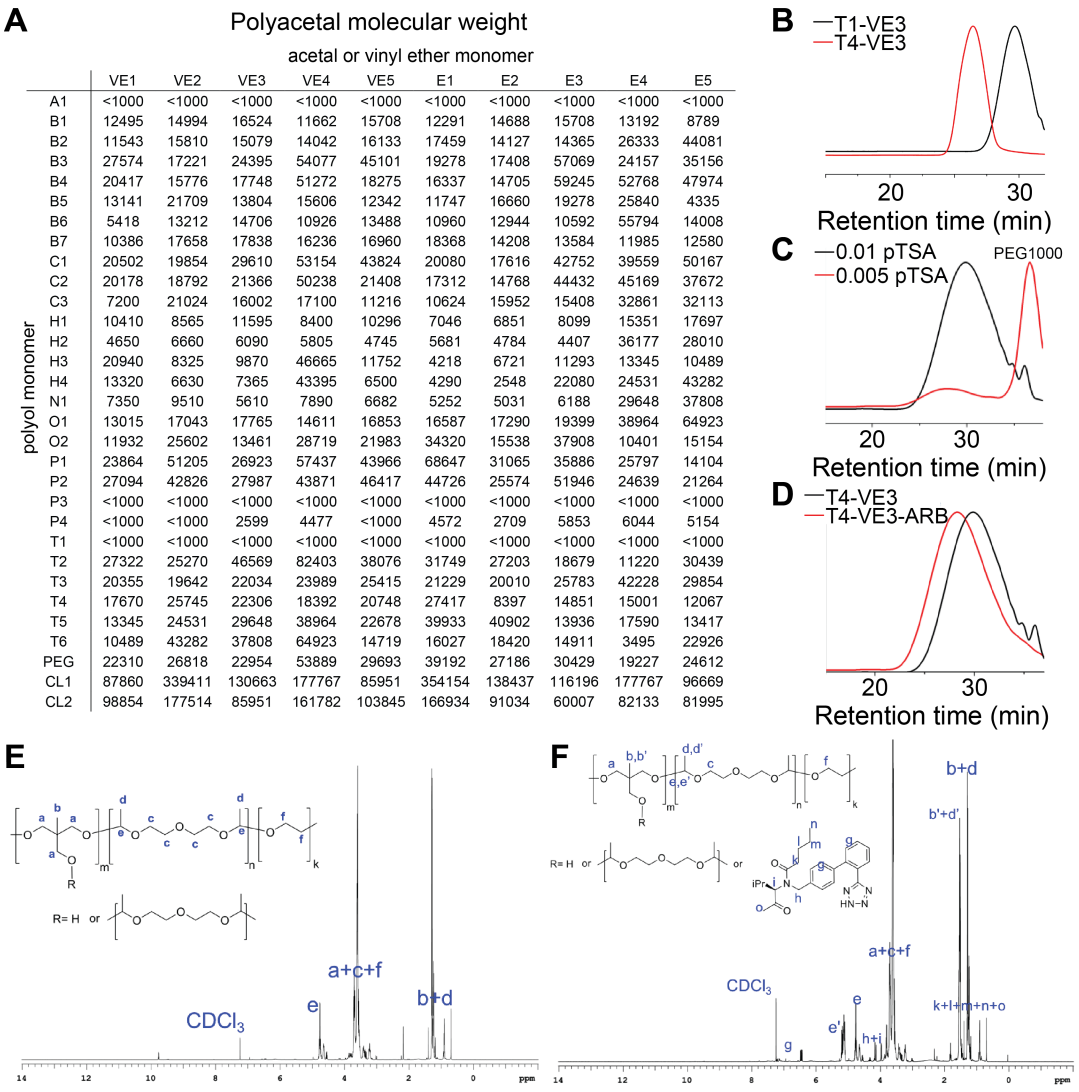

	VE1	VE2	VE3	VE4	VE5	E1	E2	E3	E4	E5
A1	<1000	<1000	<1000	<1000	<1000	<1000	<1000	<1000	<1000	<1000
B1	12495	14994	16524	11662	15708	12291	14688	15708	13192	8789
B2	11543	15810	15079	14042	16133	17459	14127	14365	26333	44081
B3	27574	17221	24395	54077	45101	19278	17408	57069	24157	35156
B4	20417	15776	17748	51272	18275	16337	14705	59245	52768	47974
B5	13141	21709	13804	15606	12342	11747	16660	19278	25840	4335
B6	5418	13212	14706	10926	13488	10960	12944	10592	55794	14008
B7	10386	17658	17838	16236	16960	18368	14208	13584	11985	12580
C1	20502	19854	29610	53154	43824	20080	17616	42752	39559	50167
C2	20178	18792	21366	50238	21408	17312	14768	44432	45169	37672
C3	7200	21024	16002	17100	11216	10624	15952	15408	32861	32113
H1	10410	8565	11595	8400	10296	7046	6851	8099	15351	17697
H2	4650	6660	6090	5805	4745	5681	4784	4407	36177	28010
H3	20940	8325	9870	46665	11752	4218	6721	11293	13345	10489
H4	13320	6630	7365	43395	6500	4290	2548	22080	24531	43282
N1	7350	9510	5610	7890	6682	5252	5031	6188	29648	37808
O1	13015	17043	17765	14611	16853	16587	17290	19399	38964	64923
O2	11932	25602	13461	28719	21983	34320	15538	37908	10401	15154
P1	23864	51205	26923	57437	43966	68647	31065	35886	25797	14104
P2	27094	42826	27987	43871	46417	44726	25574	51946	24639	21264
P3	<1000	<1000	<1000	<1000	<1000	<1000	<1000	<1000	<1000	<1000
P4	<1000	<1000	2599	4477	<1000	4572	2709	5853	6044	5154
T1	<1000	<1000	<1000	<1000	<1000	<1000	<1000	<1000	<1000	<1000
T2	27322	25270	46569	82403	38076	31749	27203	18679	11220	30439
T3	20355	19642	22034	23989	25415	21229	20010	25783	42228	29854
T4	17670	25745	22306	18392	20748	27417	8397	14851	15001	12067
T5	13345	24531	29648	38964	22678	39933	40902	13936	17590	13417
T6	10489	43282	37808	64923	14719	16027	18420	14911	3495	22926
PEG	22310	26818	22954	53889	29693	39192	27186	30429	19227	24612
CL1	87860	339411	130663	177767	85951	354154	138437	116196	177767	96669
CL2	98854	177514	85951	161782	103845	166934	91034	60007	82133	81995

Fig. S1. Structural characterization of polyacetals. (**A**) Molecular weight of each polyacetal created in the screen (in Da). Each polyacetal was created from the combination of one polyol monomer (A1-CL2) and one acetal (E1-E5) or vinyl ether (VE1-VE5) monomer (see Fig. 1). (**B-D**) Sample gel permeation chromatography (GPC) data. (**B**) Two polyacetals are shown with widely varying molecular weight: T1-VE3-PEG (M_n = 1.6 kDa) and T4-VE3-PEG (M_n = 18.2 kDa). (**C**) Low pTSA ratios resulted in insufficient PEG1000 incorporation. Excess *p*TSA resulted in a yellow-brown color shift, presumably due to the acidity of *p*TSA. (**D**) Molecular weight shift upon ARB conjugation. (**E**) The ^{1}H NMR spectrum of T4-VE3-PEG. (**F**) The ^{1}H NMR spectrum of the TMA-ARB. Peaks b, d, e in (**E**) were shifted after conjugation and are noted in (**F**) as b', d', e'.

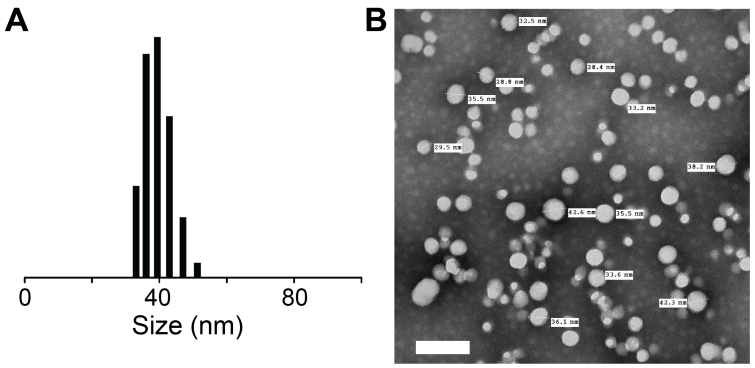

Fig. S2. Tumor microenvironment-activated ARBs form small nanoparticles. (**A**) Dynamic light scattering of the TMA-ARB. The TMA-ARB formed nanoparticles of 35 nm mean diameter. (**B**) Transmission electron microscopy of TMA-ARB nanoparticles. We applied the nanoparticle solution to a copper TEM grid, stained with 1% uranyl acetate, and dried the sample for analysis. Scale bar, 100 nm.

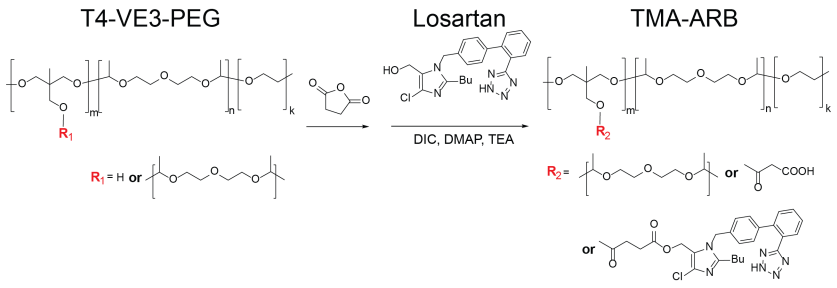

Fig. S3. Synthetic schema for conjugation of losartan to polyacetals. Conjugation of the ARB losartan to a polyacetal. The synthesis involves reaction of the polyacetal with succinic anhydride to form carboxylic acid groups through which losartan can be conjugated.

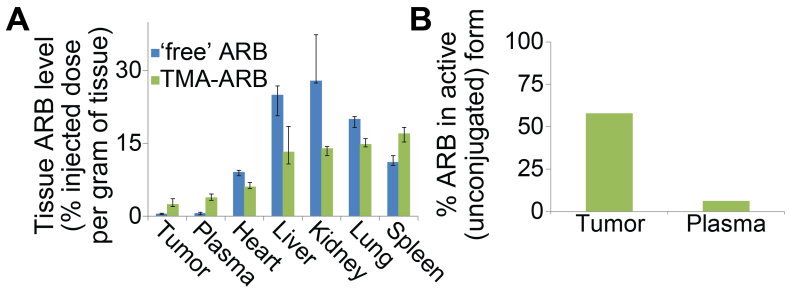

Fig. S4. Tumor-selective delivery of active ARB from the TMA-ARB. (**A**) Biodistribution of ARB in mice bearing orthotopic AK4.4 pancreatic tumors 24 hrs after intravenous injection of the 'free' ARB or the TMA-ARB at equal doses. The TMA-ARB led to tumor ARB levels 5.5-fold higher than levels achieved after injection of the 'free' ARB. Data are medians ± interquartile range. *N*=8. (**B**) Fraction of ARB found in its active (unconjugated) versus inactive (conjugated) form in mice injected with the TMA-ARB. The TMA-ARB released ARB to its active form selectively in tumors. *N*=8.

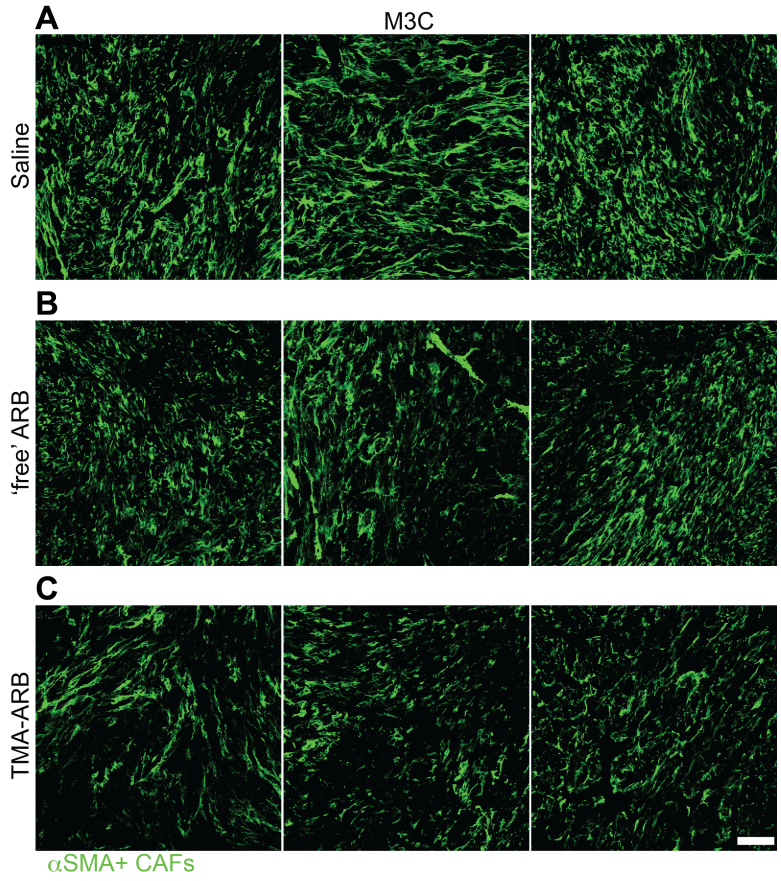

Fig. S5. Tumor microenvironment selectivity enhances CAF reprogramming by ARBs. (**A-C**) Representative images for histological analysis of tumor αSMA+ cell (primarily CAF) area fractions in orthotopic MCa-M3C breast tumors in mice treated with 'free' ARB, the TMA-ARB, or saline (control). Scale bar, 100 μm.

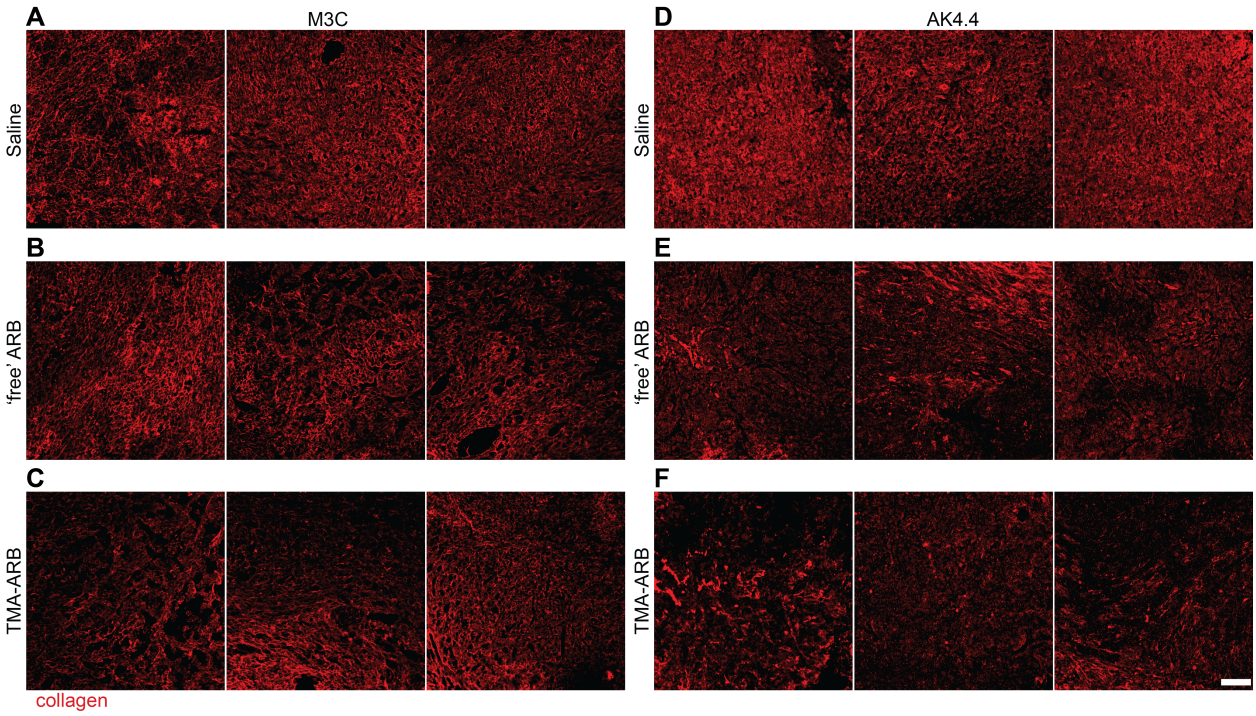

Fig. S6. Tumor microenvironment selectivity enhances collagen depletion by ARBs. Representative images for histological analysis of tumor collagen I area fractions in (**A-C**) orthotopic MCa-M3C breast tumors and (**D-F**) orthotopic AK4.4 pancreatic tumors in mice treated with 'free' ARB, the TMA-ARB, or saline (control). Scale bar, 100 μm.

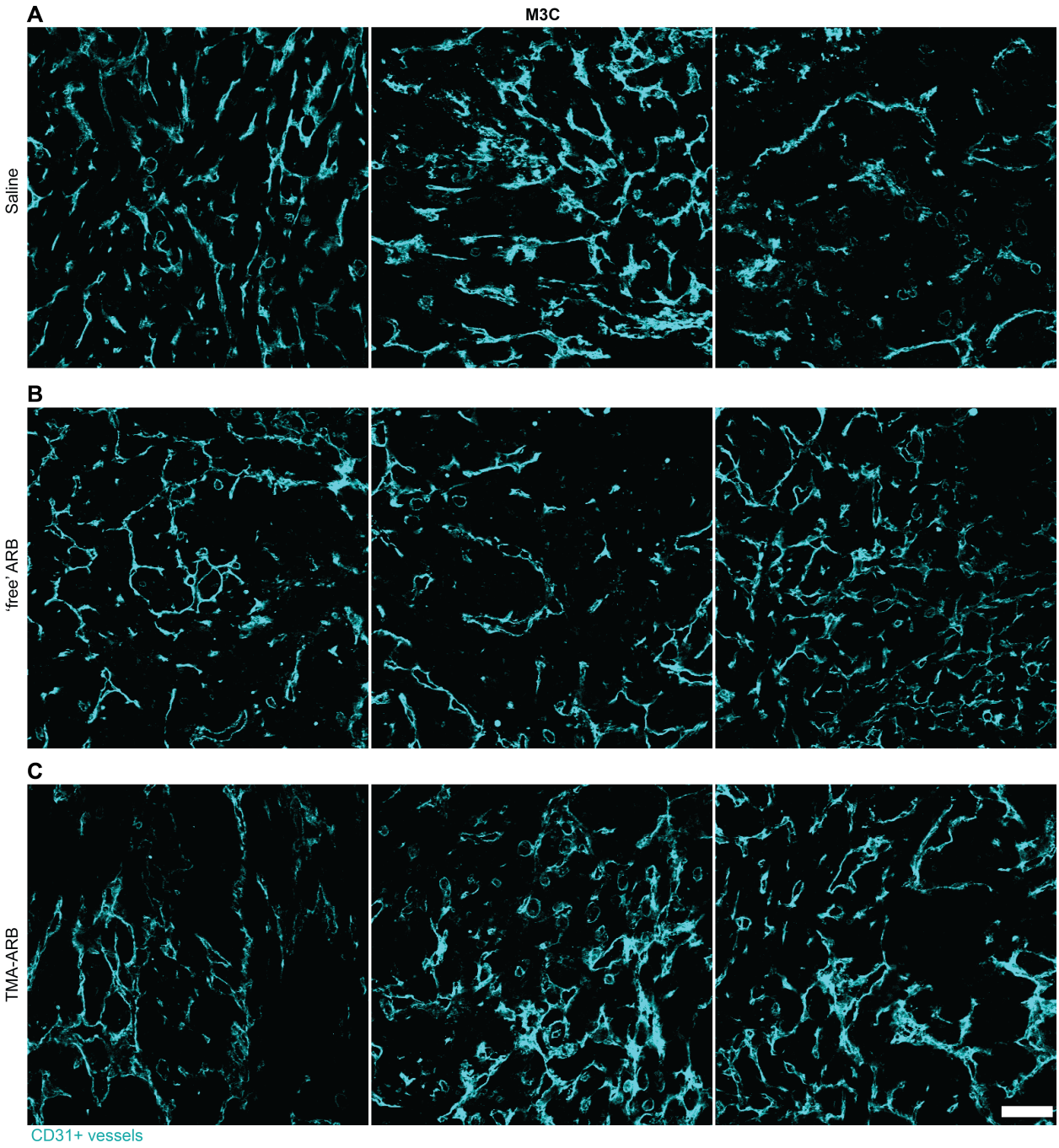

Fig. S7. Tumor microenvironment selectivity enhances vessel decompression by ARBs. (**A-C**) Representative images for histological analysis of vessel open lumen fractions in orthotopic MCa-M3C breast tumors in mice treated with 'free' ARB, the TMA-ARB, or saline (control). Open vessels are those with clearly open lumen extended along their length. The ARB treatments led to more open large vessels (rounded/elliptical structures) and small vessels (thin tubular structures with bright walls and dark lumen). Scale bar, 100 μm.

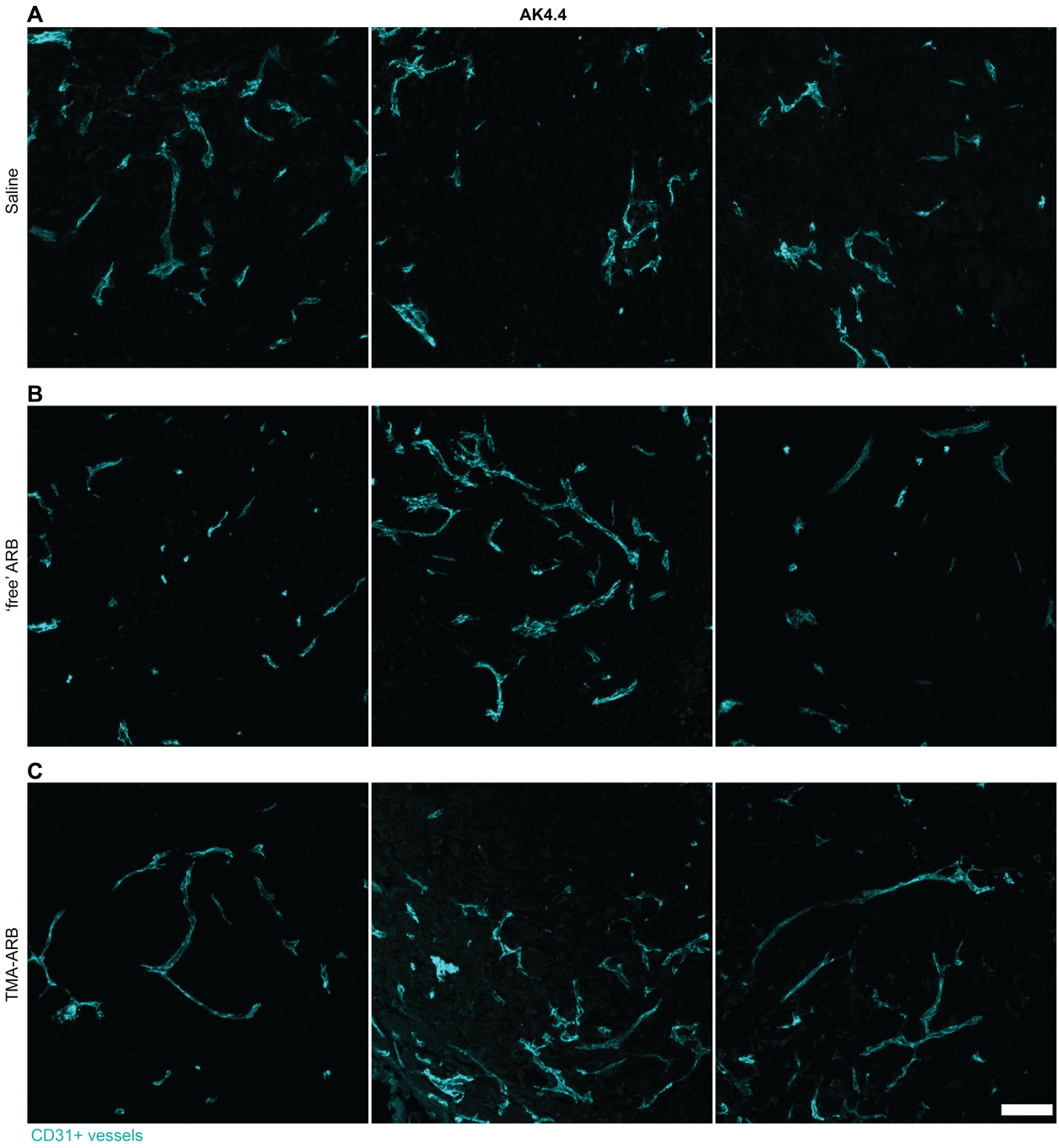

Fig. S8. Tumor microenvironment selectivity enhances vessel decompression by ARBs. (**A-C**) Representative images for histological analysis of vessel open lumen fractions in orthotopic AK4.4 pancreatic tumors in mice treated with 'free' ARB, the TMA-ARB, or saline (control). Open vessels are those with clearly open lumen extended along their length. The ARB treatments led to more open small vessels (thin tubular structures with bright walls and dark lumen). Scale bar, 100 μm.

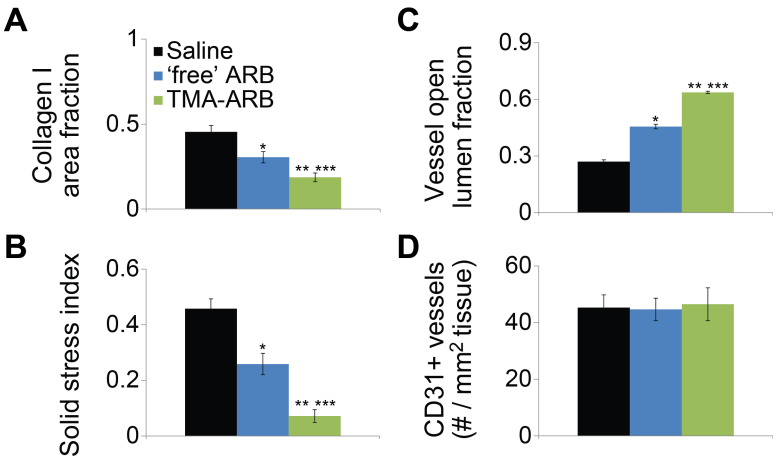

Fig. S9. Tumor microenvironment selectivity enhances normalization by ARBs. Histological and biomechanical analysis of orthotopic AK4.4 pancreatic tumors in mice treated with 'free' ARB, the TMA-ARB, or saline (control). (**A**) Tumor collagen I area fractions. Both 'free' ARB treatment (*, P=0.033) and TMA-ARB treatment (**, P<0.01) reduced tumor collagen I expression, with the TMA-ARB reducing it more (***, P=0.047). N=3-5. (**B**) Relative tumor solid stress levels. Both 'free' ARB treatment (*, P<0.01) and TMA-ARB treatment (**, P<0.01) reduced solid stress, with the TMA-ARB reducing it more (***, P<0.01). N=4-6. (**C**) Fractions of tumor blood vessels with open lumen, indicating the extent of vessel compression. Both 'free' ARB treatment (*, P<0.01) and TMA-ARB treatment (**, P<0.01) decompressed blood vessels, with the TMA-ARB most effective (***, P<0.01). N=4. (**D**) Tumor blood vessel density. N=4.

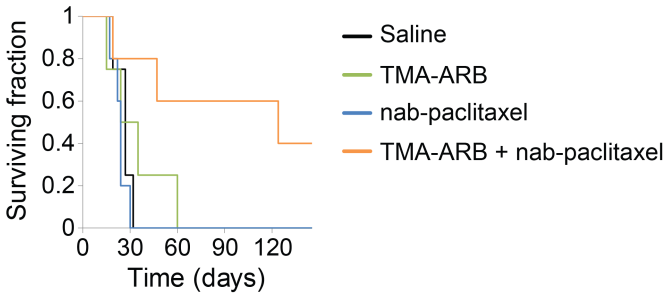

Fig. S10. TMA-ARBs enhance chemotherapy in breast cancer. Metastatic setting animal survival studies in mice with spontaneous lung metastases arising from orthotopic MCa-M3C breast tumors treated with chemotherapy in combination with the TMA-ARB. Following resection of the primary tumors to leave only the metastatic disease, mice were treated with the TMA-ARB or saline (control) on days 0-5, and with or without the chemotherapeutic nab-paclitaxel on days 2-6. The chemotherapy alone did not extend animal survival, yet the combination with the TMA-ARB improved animal survival by 359% versus the controls (P=0.040) and by 417% versus the immunotherapy cocktail alone (P=0.029). N=4-5.

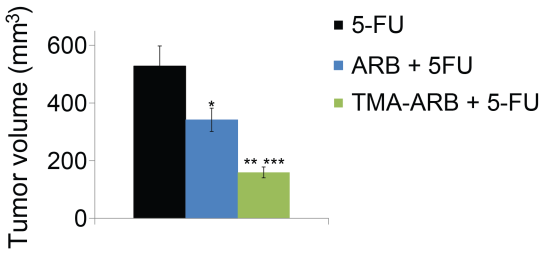

Fig. S11. TMA-ARBs enhance chemotherapy in pancreatic cancer. Primary tumor growth studies in mice bearing orthotopic AK4.4 pancreatic tumors treated with chemotherapy in combination with the 'free' ARB or TMA-ARB. Mice were treated with the TMA-ARB, 'free' ARB, or saline (control) on days 1-12 following tumor implantation, and with or without the chemotherapeutic 5-fluorouracil (5-FU) on days 5, 9 and 13. Tumors were measured on day 14. The ARB improved the outcome of chemotherapy (*, P=0.05), as did the TMA-ARB (**, P<0.01), though the TMA-ARB enhanced chemotherapy to a greater degree (***, P<0.01). N=5-6.

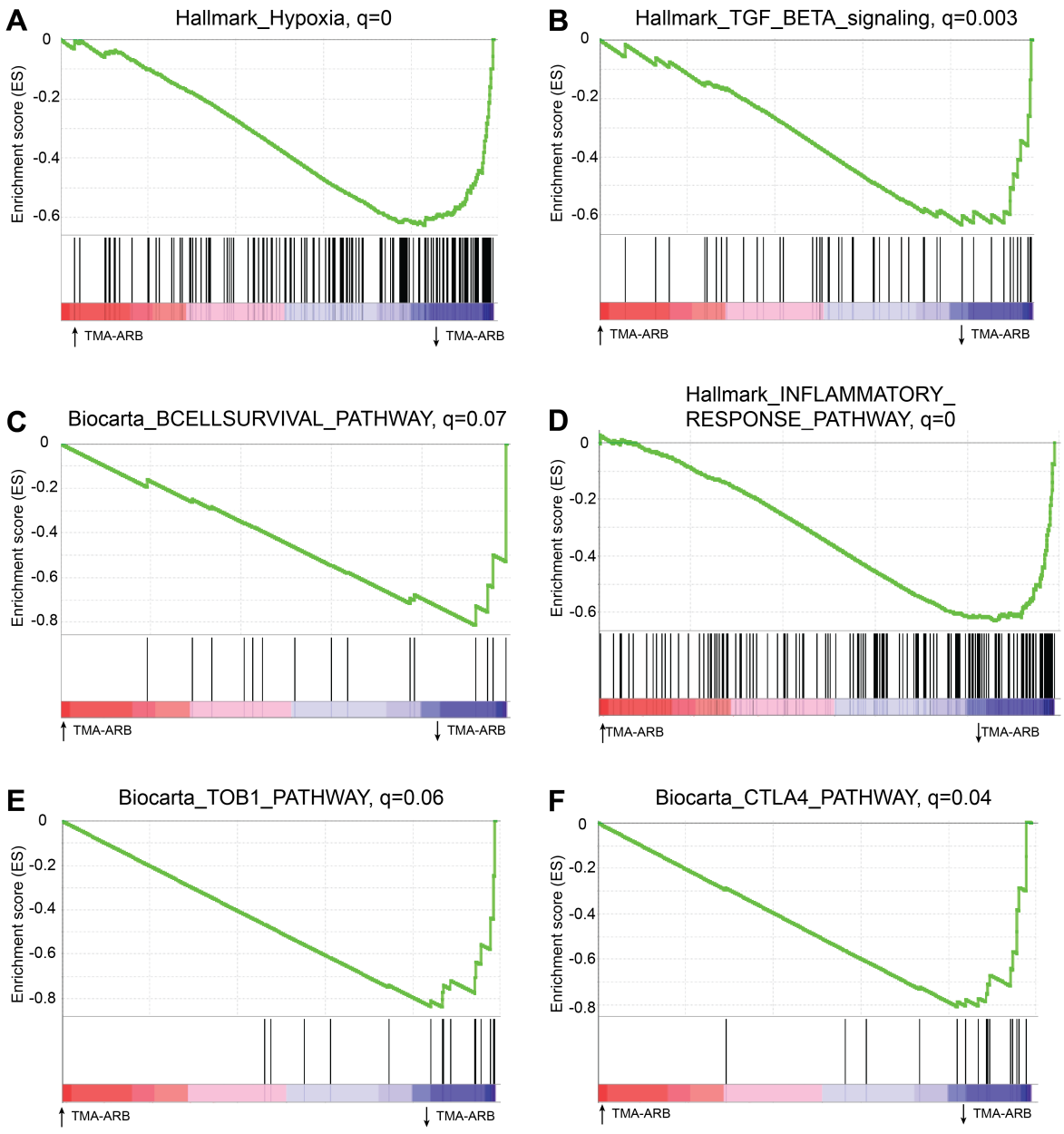

Fig. S12. TMA-ARB treatment inhibits multiple immunosuppressive pathways in breast tumors. (**A-F**) Enrichment plots showing pathways from the MSigDB Hallmarks and Biocarta collections that were significantly down-regulated in TMA-ARB treated tumors. All depicted gene sets were among the top ten hits in both collections and had a false discovery rate (FDR) below 10%. TMA-ARB treatment down-regulated genes related to (**A**) hypoxia, (**B**) TGF-β, (**C**) B cell survival, (**D**) inflammatory response, (**E**) TOB1, and (**F**) CTLA4 signaling.

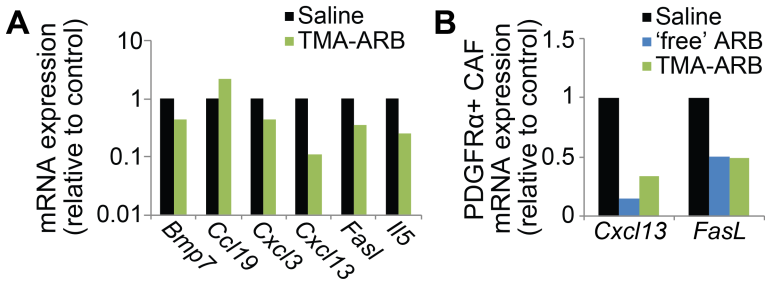

Fig. S13. TMA-ARB treatment reduces expression of immunosuppressive genes. Gene expression analysis by qRT-PCR in orthotopic MCa-M3C breast tumors in mice treated with the TMA-ARB or saline (control). (**A**) Hits from a gene array for cytokines, chemokines, and related genes for pooled whole tumor lysates from mice treated with the TMA-ARB vs saline. Pooled from *N*=4-8. (**B**) Gene expression in PDGFRα+ CAFs sorted from MCa-M3C tumors. Treatment with the ARB and TMA-ARB decreased *Cxcl13* and *Fasl* expression in these sorted CAFs. Pooled from *N*=4.

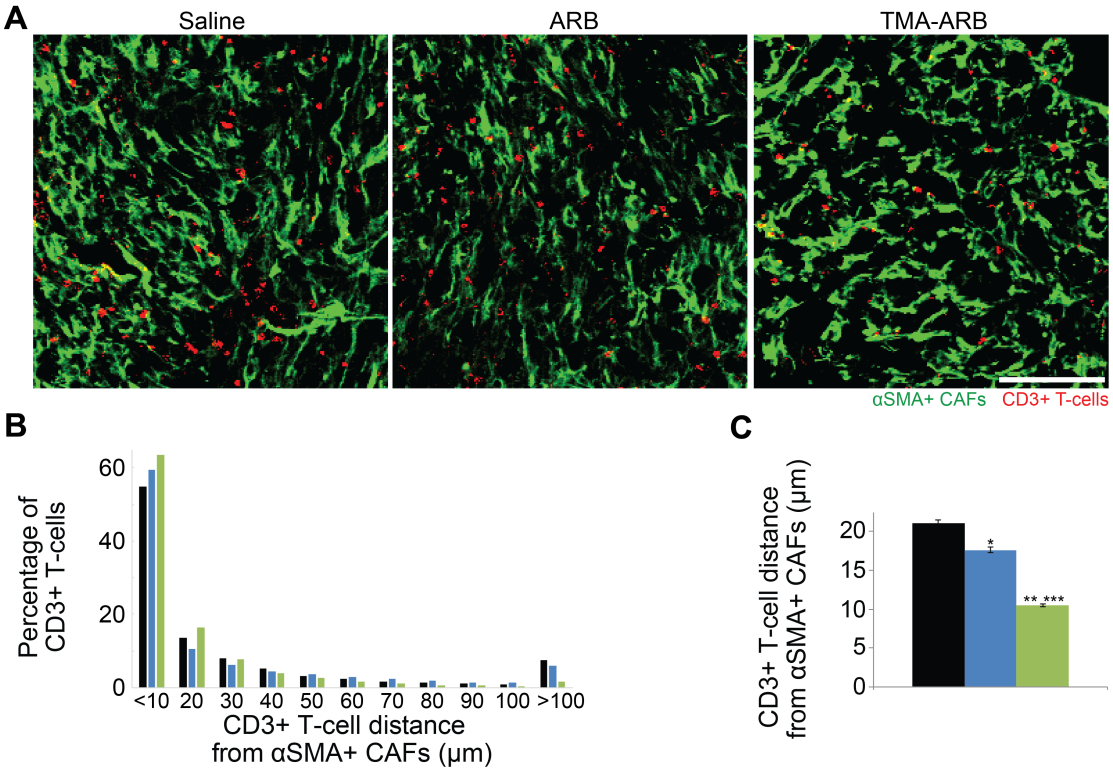

Fig. S14. TMA-ARB treatment enhances T-lymphocyte penetration in CAF-rich tumors. Histological analysis of T cell distribution in orthotopic MCa-M3C breast tumors in mice treated with 'free' ARB, the TMA-ARB, or saline (control). (**A**) Representative histological images of CD3+ T cell (red) infiltration distance relative to αSMA+ cells (primarily CAFs, green). Scale bar, 100 μm. (**B**) Histogram of the distance between each CD3+ T cell and its nearest αSMA+ cell (pooled from *N*=6-8 tumors, 8 images per tumor). (**C**) Mean distance between CD3+ T cells and αSMA+ cells. ARB and TMA-ARB treatment decreased the distance between T cells and αSMA+ cells (* ** ***, $P<0.01$).

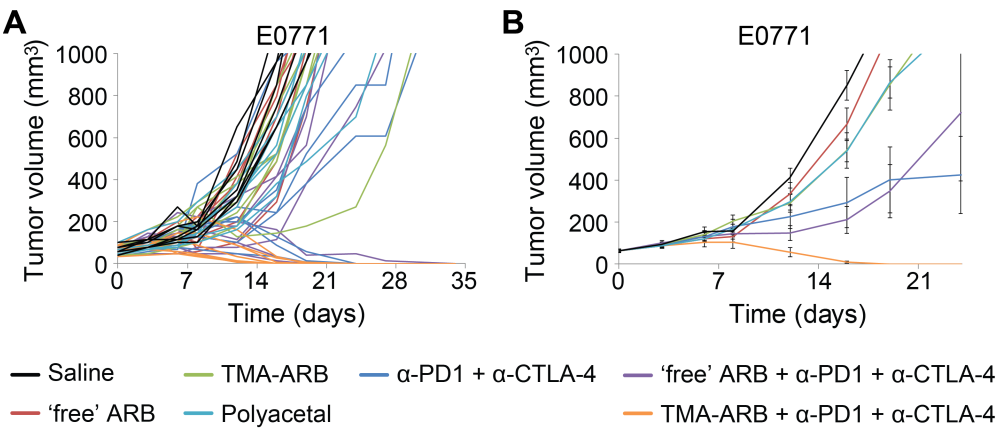

Fig. S15. Tumor microenvironment selectivity enables the enhancement of immune checkpoint blocker outcomes by ARBs. Primary tumor growth studies in mice bearing orthotopic E0771 breast tumors treated with immune checkpoint blockers in combination with the 'free' ARB or TMA-ARB nanoconjugates. Mice were treated with the 'free' ARB, TMA-ARB, unconjugated polyacetal, or saline (control) on days 0-7, and with or without a cocktail of immune checkpoint blocking antibodies against cytotoxic T-lymphocyte-associated protein 4 (α-CTLA-4) and programmed cell death 1 (α-PD-1) on days 2, 5, and 8. (**A**) Individual tumor growth curves. The 'free' ARB, TMA-ARB, and polyacetal monotherapies did not affect growth. The immunotherapy cocktail alone or in combination with the 'free' ARB caused regression and cures in 3 of 7 tumors, while the combination with the TMA-ARB caused regression and cures in 7 of 7 mice. (**B**) Mean tumor growth curves. The 'free' ARB combined with the immunotherapy cocktail did not significantly improve growth delay when compared with the immunotherapy cocktail alone, while the TMA-ARB combined with the immunotherapy cocktail improved growth delay versus the other groups (P<0.01). N=7.

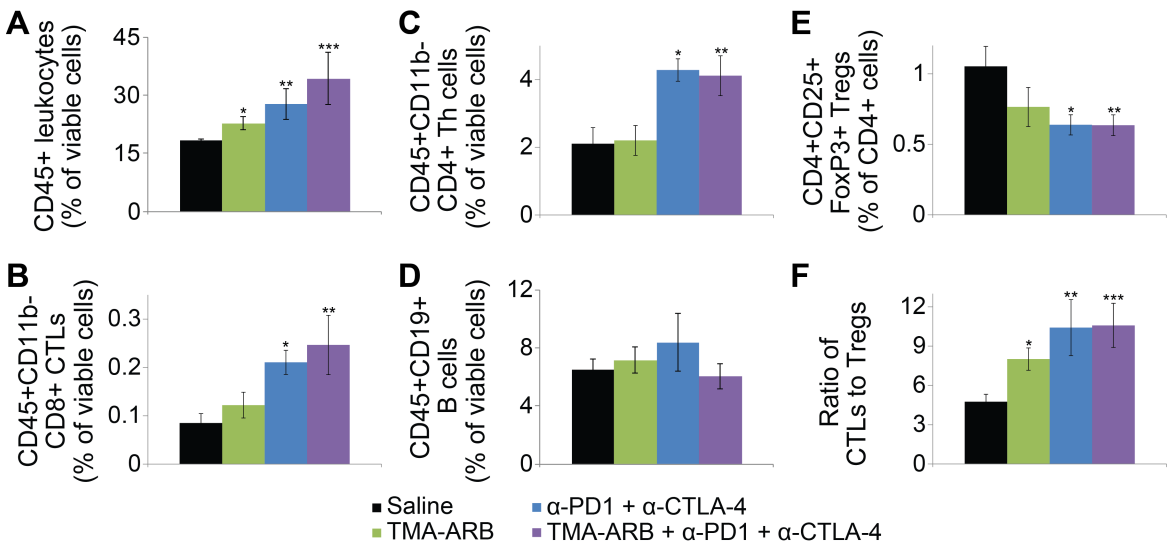

Fig. S16. TMA-ARB treatment increases leukocyte infiltration and the cytotoxic to regulatory T-lymphocyte ratio. Flow cytometry analysis of adaptive leukocyte populations from orthotopic E0771 breast tumors in mice treated with the TMA-ARB in combination with a cocktail of a blocking antibody against cytotoxic T-lymphocyte-associated protein 4 (α-CTLA-4) and a blocking antibody against programmed cell death 1 (α-PD-1). (**A**) CD45+ (leukocyte) cell fractions. The TMA-ARB (*, P=0.030), the immunotherapy cocktail (**, P=0.036), and the combination with the TMA-ARB (***, P=0.038) increased CD45+ cell fractions. N=6. (**B**) CD45+CD11b-CD8+ (cytotoxic T-lymphocyte) cell fractions. Again, the immunotherapy cocktail (*, P<0.01) and the combination with the TMA-ARB (**, P=0.031) increased CD45+CD11b-CD8+ cell fractions. N=6. (**C**) CD45+CD11b-CD4+ (helper T-lymphocyte) cell fractions. Similarly, the immunotherapy cocktail (*, P<0.01) and the combination with the TMA-ARB (**, P=0.024) both increased CD45+CD11b-CD4+ cell fractions. N=6. (**D**) CD45+CD19+ (B-lymphocyte) cell fractions. No changes were observed. N=6. (**E**) CD45+CD11b-CD4+CD25+FoxP3+ (regulatory T-lymphocyte) cell fractions. Both the immunotherapy cocktail (*, P=0.026) and the combination with the TMA-ARB (**, P=0.026) decreased CD45+CD11b-CD4+CD25+FoxP3+ cell fractions. N=6. (**F**) Ratio of CD45+CD11b-CD8+ to CD45+CD11b-CD4+CD25+FoxP3+ cells. The ratio was increased by the TMA-ARB (*, P=0.020), the immunotherapy cocktail (**, P=0.028), and the combination (***, P=0.025).

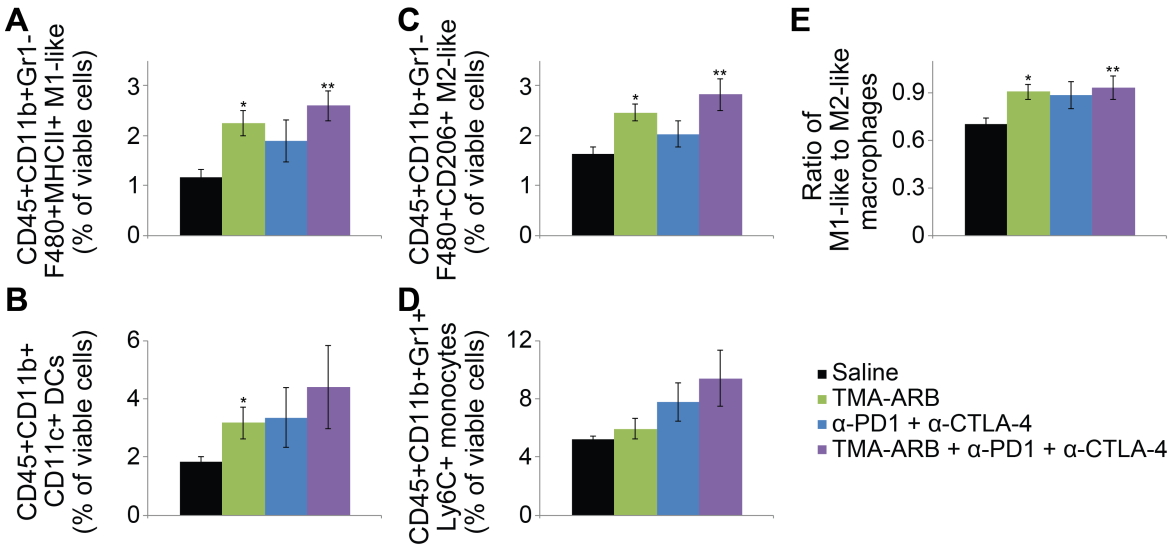

Fig. S17. TMA-ARB treatment increases dendritic cell populations and polarizes macrophages toward an anti-tumor phenotype. Flow cytometry analysis of innate leukocyte populations from orthotopic E0771 breast tumors in mice treated with the TMA-ARB in combination with a cocktail of a blocking antibody against cytotoxic T-lymphocyte-associated protein 4 (α-CTLA-4) and a blocking antibody against programmed cell death 1 (α-PD-1). (**A**) CD45+CD11b+Gr1-F480+MHCII+ (M1-like macrophage) cell fractions. Both the TMA-ARB (*, P<0.01) and the combination of the immunotherapy cocktail with the TMA-ARB (**, P<0.01) increased CD45+CD11b+Gr1-F480+MHCII+ cell fractions. N=6. (**B**) CD45+CD11b+CD11c+ (dendritic cell) cell fractions. The TMA-ARB (*, P=0.040) increased CD45+CD11b+CD11c+ cell fractions. N=6. (**C**) CD45+CD11b+Gr1-F480+CD206+ (M2-like macrophage) cell fractions. Again, the TMA-ARB (*, P<0.01) and the combination of the immunotherapy cocktail with the TMA-ARB (**, P<0.01) increased CD45+CD11b+Gr1-F480+CD206+ cell fractions. N=6. (**D**) CD45+CD11b+Gr1+Ly6C+ (monocyte) cell fractions. No changes were observed. N=6. (**E**) Ratio of CD45+CD11b+Gr1-F480+MHCII+ to CD45+CD11b+Gr1-F480+CD206+ cells. The M1-like to M2-like ratio was increased by the TMA-ARB (*, P<0.01) and the combination (**, P=0.021).

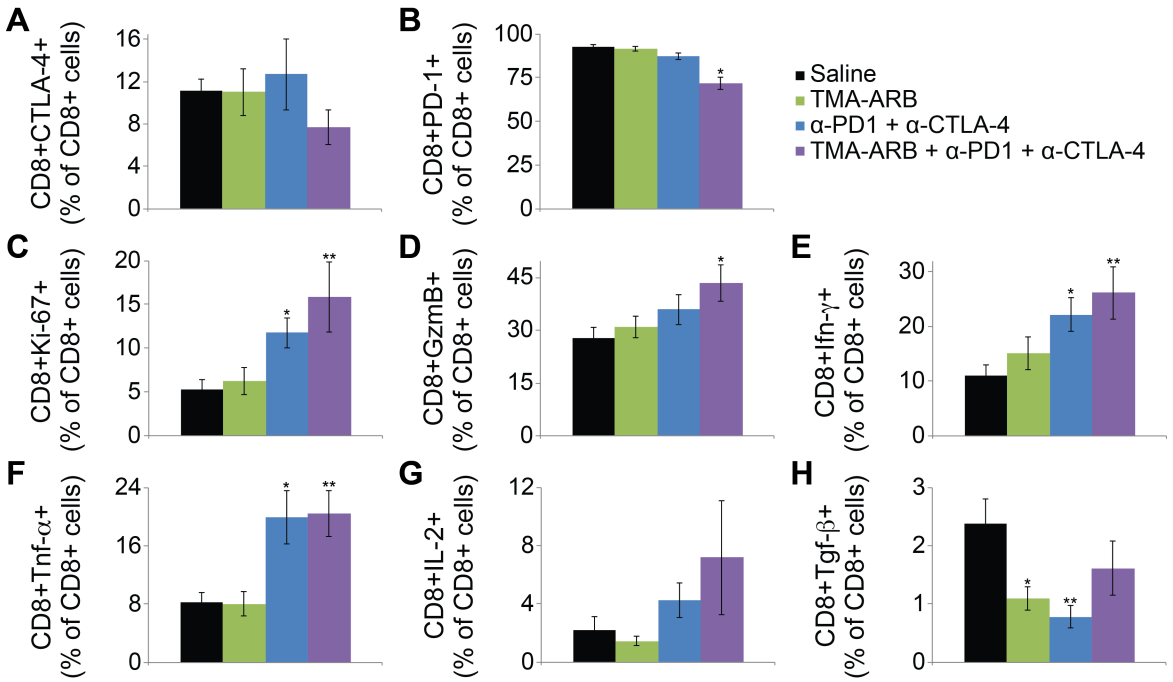

Fig. S18. TMA-ARB treatment combined with immune checkpoint blockers increases T-lymphocyte activity and decreases dysfunction. Flow cytometry analysis of markers of cytotoxic T-lymphocyte activation in orthotopic E0771 breast tumors in mice treated with the TMA-ARB in combination with a cocktail of a blocking antibody against cytotoxic T-lymphocyte-associated protein 4 (α-CTLA-4) and a blocking antibody against programmed cell death 1 (α-PD-1). (**A**) Fraction of cells expressing CTLA-4. No effect. *N*=6. (**B**) Fraction of cells expressing PD-1. The combination of the immunotherapy cocktail and the TMA-ARB decreased PD-1 expression (*, *P*<0.01), indicating decreased dysfuntion. *N*=6. (**C**) Fraction of cells expressing Ki-67. Both the immunotherapy cocktail (*, *P*=0.010) and the combination with the TMA-ARB (**, *P*=0.030) increased Ki-67 expression, indicating increased proliferation. *N*=6. (**D**) Fraction of cells expressing Granzyme B. The combination therapy increased GzmB expression (*, *P*=0.027), indicating increased activity. *N*=6. (**E**) Fraction of cells expressing Interferon-γ. Both the immunotherapy cocktail (*, *P*=0.013) and the combination with the TMA-ARB (**, *P*=0.015) increased Ifn-γ expression, indicating increased activation. *N*=6. (**F**) Fraction of cells expressing Tumor necrosis factor α. Both the immunotherapy cocktail (*, *P*=0.013) and the combination with the TMA-ARB (**, *P*<0.01) increased Tnf-α expression, indicating increased activation. *N*=6. (**G**) Fraction of cells expressing Interleukin-2. No effect. *N*=6. (**H**) Fraction of cells expressing Tumor growth factor β. The TMA-ARB (*, *P*=0.019) and the immunotherapy cocktail (**, *P*<0.01) decreased TGF-β expression, indicating decreased dysfunction. *N*=6.

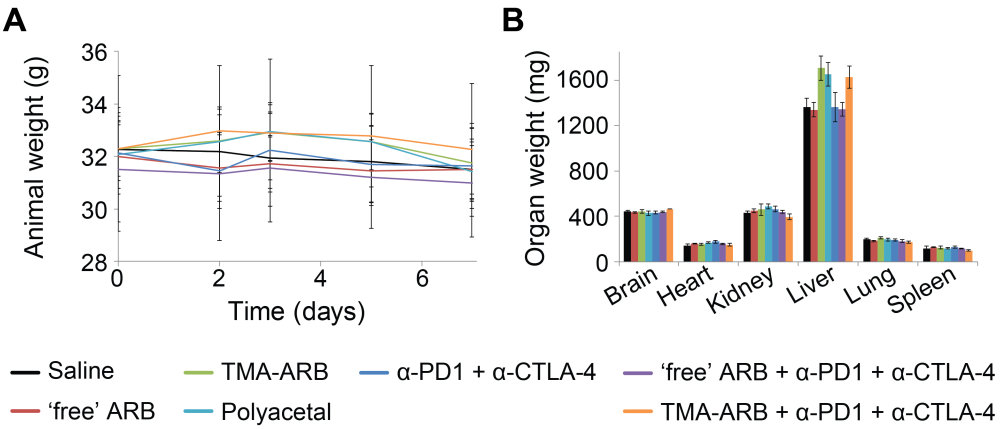

Fig. S19. Treatment with ARBs and immune checkpoint blockers does not affect animal weight. Measurements of animal weight over the course of treatment of FVB mice on the schedules as in the tumor growth and animal survival studies. (**A**) Animal weights. (**B**) Organ weights at the termination of treatment (day 9). None of the treatments affected animal or organ weights significantly. *N*=5.

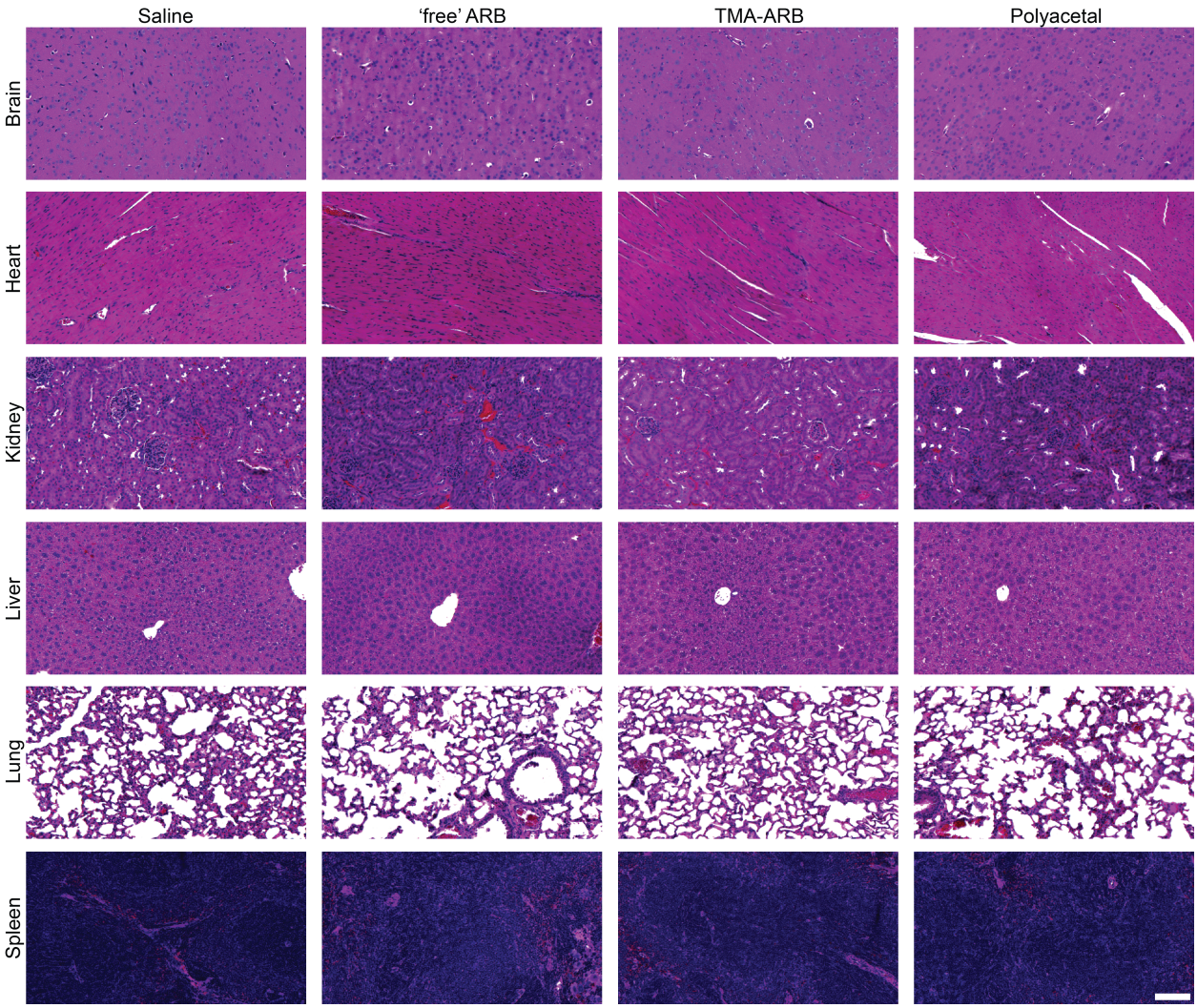

Fig. S20. Treatment with ARBs does not induce tissue toxicity. Representative images for histological analysis of tissue toxicity at the termination of treatment of FVB mice on the schedules as in the tumor growth and animal survival studies. None of the treatments induced observable tissue toxicity. *N*=5. Scale bar, 100 μm.

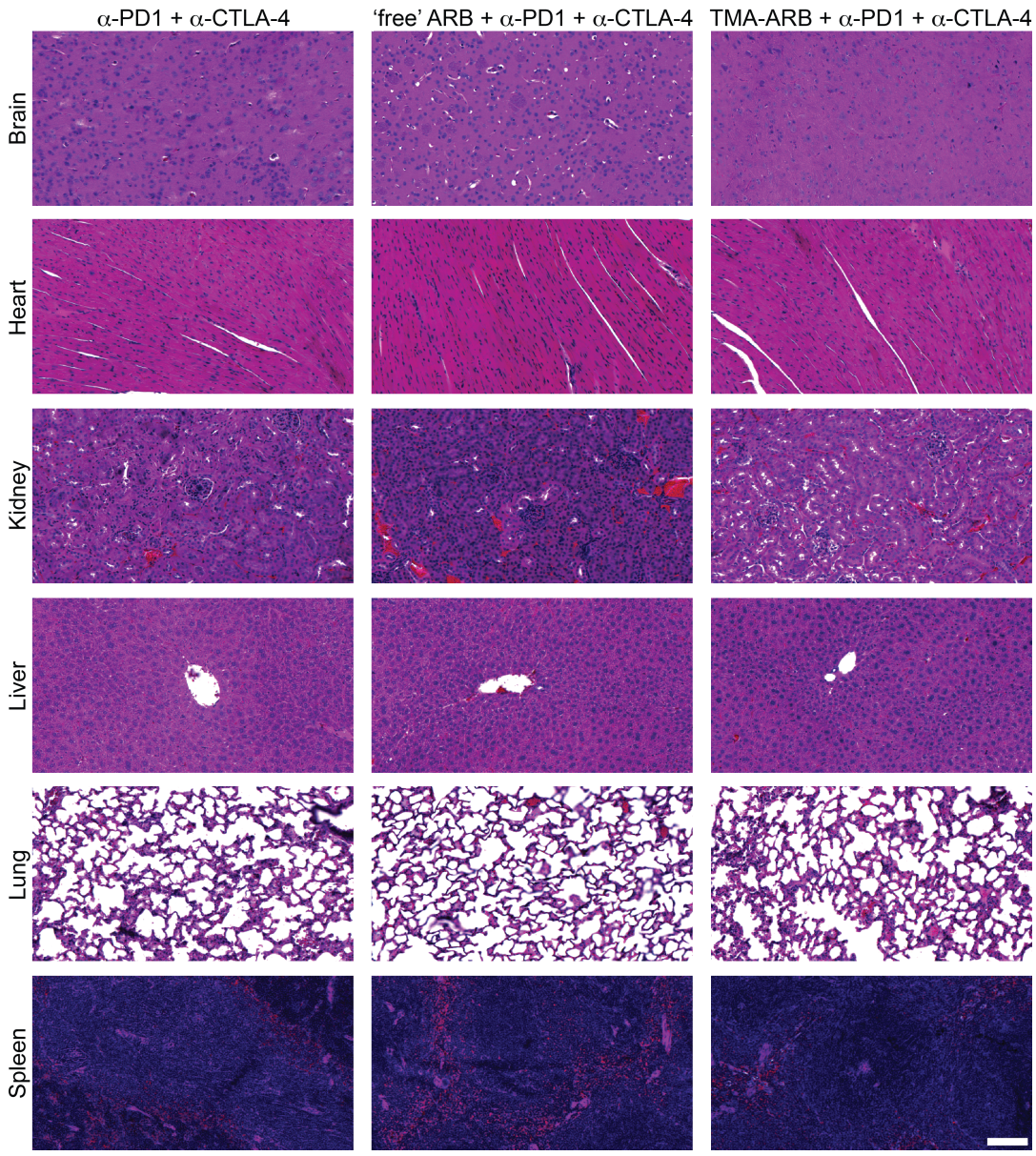

Fig. S21. Treatment with ARBs and immune checkpoint blockers does not induce tissue toxicity. Representative images for histological analysis of tissue toxicity at the termination of treatment of FVB mice on the schedules as in the tumor growth and animal survival studies. None of the treatments induced observable tissue toxicity. *N*=5. Scale bar, 100 μm.

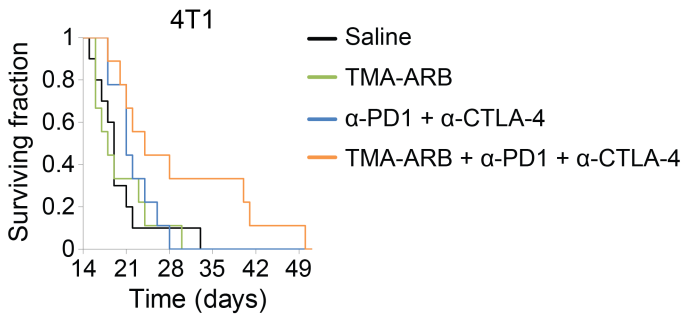

Fig. S22. TMA-ARBs enhance immune checkpoint blockers. Repeated study of animal survival in mice with spontaneous metastases from 4T1 primary tumors treated with immune checkpoint blockers in combination with the TMA-ARB. Mice were treated with the TMA-ARB or saline (control) on days 0-7, and with or without a cocktail of immune checkpoint blocking antibodies against cytotoxic T-lymphocyte-associated protein 4 (α-CTLA-4) and programmed cell death 1 (α-PD-1) on days 2, 5, and 8. The immunotherapy cocktail did not extend animal survival, meanwhile the combination with the TMA-ARB improved animal survival by 26% versus the controls (P=0.0453). N=9-10.

Supporting Tables

Trial	Drug	Sponsor	Phase	Results	Reference
NCT01848834 (KEYNOTE-012)	α-PD-1	Merck	1b	27 TNBC pts (ORR 19%)	Nanda et al. (7)
NCT01375842	α-PD-L1	Genentech	1	24 TNBC pts (ORR 24%)	Emens et al. (8)
NCT01633970	α-PD-1, nab-paclitaxel	Genentech	1	24 TNBC pts (ORR 42%)	Adams et al. (9)
NCT01772004 (JAVELIN)	α-PD-L1	EMD Serono, Merck	1	168 pts (ORR 5.2%; 8.6% TNBC, 4.2% ER+/HER2-)	Dirix et al. (10)
NCT02054806(KEYNOTE-028)	α-PD-1	Merck	1	25 ER+/HER2- pts (ORR 12%)	Rugo et al. (11)

Table S1. Clinical trials of immune checkpoint blockers in breast cancer. Preliminary results from early trials. The number of patients (pts) in each trial, the breast cancer subtype (triple-negative, TNBC; estrogen receptor-positive, ER+; human epidermal growth factor receptor 2 negative; HER2-), and the overall response rate (ORR) are listed for each trial.

	Saline	'free' ARB	TMA-ARB	Polyacetal	α-PD1 + α-CTLA-4	'free' ARB + α-PD1 + α-CTLA-4	TMA-ARB + α-PD1 + α-CTLA-4
White blood cells (10^3/μL)	5.3 ± 1.1	5.42 ± 2.0	4.7 ± 0.3	4.8 ± 1.6	4.1 ±1.1	4.3 ± 1.2	5.1 ± 0.9
Lymphocytes (10^3/μL)	4.1 ± 0.8	4.2 ± 1.6	3.7 ± 0.5	3.6 ± 1.1	3.0 ± 0.9	3.2 ± 1.1	4.0 ± 0.6
Monocytes (10^3/μL)	0.3 ± 0.1	0.3 ± 0.1	0.3 ± 0.1	0.3 ± 0.1	0.24 ± 0.1	0.3 ± 0.0	0.3 ± 0.1
Granulocytes (10^3/μL)	0.8 ± 0.3	0.9 ± 0.3	0.8 ± 0.3	0.9 ± 0.5	0.8 ± 0.2	0.8 ± 0.1	0.8 ± 0.2
Lymphocytes (%)	78.2 ± 2.1	77.5 ± 1.8	77.8 ± 7.2	75.0 ± 3.8	74.4 ± 3.3	74.4 ± 2.6	78.1 ± 1.8
Monocyte (%)	5.3 ± 0.7	4.9 ± 0.5	5.4 ± 1.0	6.0 ± 1.1	5.6 ± 0.9	5.1 ± 0.8	5.1 ± 0.5
Granulocyte (%)	16.4 ± 2.8	17.7 ± 1.4	16.8 ± 6.4	19.0 ± 2.7	20.1 ± 2.6	20.6 ± 1.8	16.8 ± 1.4
Hematocrit (%)	49.5 ± 9.2	46.5 ± 4.7	41.8 ± 9.5	45.8 ± 6.3	45.8 ± 4.6	46.7 ± 2.1	44.0 ± 2.6
Mean corpuscular volume (fL)	48.1 ± 0.5	48.4 ± 0.3	48.7 ± 0.5	49.2 ± 0.3	48.9 ± 1.4	48.7 ± 1.2	48.7 ± 0.3
Red cell distribution width (fL)	32.8 ± 0.2	33.2 ± 0.6	32.7 ± 0.8	33.4 ± 0.9	34.2 ± 2.4	33.5 ± 1.2	31.9 ± 0.2
Red cell distribution width (%)	16.0 ± 0.1	16.2 ± 0.5	16.0 ± 0.6	15.9 ± 0.5	16.5 ± 0.7	16.0 ± 0.3	15.2 ± 0.4
Hemoglobin (g/dL)	15.5 ± 2.8	14.7 ± 1.5	13.4 ± 2.8	14.4 ± 1.8	14.5 ± 1.3	14.6 ± 0.6	13.7 ± 1.0
Mean cell hemoglobin conc. (g/dL)	31.3 ± 0.3	31.7 ± 0.3	32.1 ± 0.8	31.5 ± 0.9	31.7 ± 0.5	31.3 ± 0.3	31.1 ± 0.5
Mean cell hemoglobin (Pg)	15.0 ± 0.3	15.3 ± 0.1	15.6 ± 0.6	15.5 ± 0.5	15.5 ± 0.4	15.2 ± 0.6	15.2 ± 0.2
Red blood cell (10^6/μL)	10.3 ± 2.0	9.6 ± 1.0	8.6 ± 2.0	9.3 ± 1.3	9.4 ± 0.9	9.6 ± 0.7	9.0 ± 0.6
Platelet (10^3/μL)	571.7 ± 356.6	545.8 ± 249.7	733.3 ± 232.8	784.8 ± 111.0	860.0 ± 154.7	588.0 ± 84.9	641.0 ± 230.2
Mean platelet volume (fL)	6.6 ± 0.2	7.1 ± 0.0	7.1 ± 0.6	7.0 ± 0.3	7.0 ± 0.3	7.5 ± 1.0	7.0 ± 0.5
Albumin (g/dL)	2.0 ± 0.6	2.3 ± 0.3	2.0 ± 0.2	2.1 ± 0.3	2.1 ± 0.6	2.7 ± 0.7	2.4 ± 0.5
Alkaline phosphatase (U/L)	72.2 ± 12.9	74.2 ± 9.8	68.8 ± 16.6	67.8 ± 13.5	68.2 ± 10.6	79.6 ± 15.2	66.6 ± 18.0
ALT (GPT) (U/L)	77.2 ± 27.9	88.0 ± 53.6	105.6 ± 124.1	95.8 ± 79.6	139.4 ± 227.9	405.4 ± 311.4	119 ± 102.2
BUN (mg/dL)	23.7 ± 1.2	24.6 ± 2.0	23.9 ± 4.5	24.1 ± 2.7	22.0 ± 1.7	24.4 ± 1.3	25.1 ± 2.3
Calcium (mg/dL)	8.7 ± 0.5	8.9 ± 0.3	9.2 ± 0.4	9.4 ± 0.1	9.2 ± 0.7	8.8 ± 0.4	9.0 ± 0.6
Cholesterol (mg/dL)	166 ± 23.4	185.8 ± 11.8	175.4 ± 13.4	186.5 ± 8.8	172.6 ± 32.2	173.6 ± 21.9	170.6 ± 37.0
Creatinine (mg/dL)	0.2 ± 0.0	0.2 ± 0.0	0.3 ± 0.1	0.2 ± 0.0	0.2 ± 0.1	0.3 ± 0.1	0.2 ± 0.0
Globulin (g/dL)	2.7 ± 0.4	2.8 ± 0.3	2.7 ± 0.1	2.8 ± 0.1	2.7 ± 0.3	2.9 ± 0.4	2.7 ± 0.5
Glucose (mg/dL)	226.8 ± 55.3	194.2 ± 68.4	174.0 ± 60.3	177.3 ± 43.1	160.4 ± 49.1	293.8 ± 117.0	190.0 ± 62.0
Phosphorus (mg/dL)	6.8 ± 0.6	7.0 ± 0.7	8.2 ± 1.5	8.1 ± 1.0	8.4 ± 1.2	9.7 ± 1.1	7.9 ± 1.6
Total Bilirubin (mg/dL)	1.1 ± 1.3	1.0 ± 0.5	0.5 ± 0.3	0.4 ± 0.3	0.4 ± 0.2	2.3 ± 1.4	1.2 ± 0.8
Total Protein (g/dL)	4.7 ± 1.0	5.1 ± 0.5	4.7 ± 0.3	4.9 ± 0.4	4.8 ± 0.9	5.7 ± 1.1	5.0 ± 1.0

Table S2. Treatment with ARBs and immune checkpoint blockers does not induce tissue toxicity. Clinical chemistry analysis of tissue toxicity at the termination of treatment of FVB mice on the schedules as in the tumor growth and animal survival studies. None of the treatments induced significant tissue toxicity, though some of the mice in the immunotherapy groups had high ALT levels. *N*=4-5.

Supporting References

1. Nia HT*, et al.* (2016) Solid stress and elastic energy as measures of tumour mechanopathology. *Nature Biomedical Engineering* 1:0004.
2. Chauhan VP*, et al.* (2013) Angiotensin inhibition enhances drug delivery and potentiates chemotherapy by decompressing tumour blood vessels. *Nature Communications* 4:2516.
3. Padera TP*, et al.* (2004) Pathology: cancer cells compress intratumour vessels. *Nature* 427(6976):695.
4. Stylianopoulos T*, et al.* (2012) Causes, consequences, and remedies for growth-induced solid stress in murine and human tumors. *Proceedings of the National Academy of Sciences of the United States of America* 109(38):15101-15108.
5. Robinson MD, McCarthy DJ, & Smyth GK (2010) edgeR: a Bioconductor package for differential expression analysis of digital gene expression data. *Bioinformatics (Oxford, England)* 26(1):139-140.
6. Subramanian A*, et al.* (2005) Gene set enrichment analysis: a knowledge-based approach for interpreting genome-wide expression profiles. *Proceedings of the National Academy of Sciences of the United States of America* 102(43):15545-15550.
7. Nanda R*, et al.* (2016) Pembrolizumab in Patients With Advanced Triple-Negative Breast Cancer: Phase Ib KEYNOTE-012 Study. *Journal of Clinical Oncology* 34(21):2460-2467.
8. Emens LA*, et al.* (2015) Inhibition of PD-L1 by MPDL3280A leads to clinical activity in patients with metastatic triple-negative breast cancer (TNBC). *Cancer Research* 75(15 Supplement):2859-2859.
9. Adams S*, et al.* (2015) Safety and clinical activity of atezolizumab (anti-PDL1) in combination with nab-paclitaxel in patients with metastatic triple-negative breast cancer. *Proceedings of the Thirty-Eighth Annual CTRC-AACR San Antonio Breast Cancer Symposium*, pp 6-10.
10. Dirix L*, et al.* (2016) Avelumab (MSB0010718C), an anti-PD-L1 antibody, in patients with locally advanced or metastatic breast cancer: A phase Ib JAVELIN solid tumor trial. *Cancer Research* 76(4 Supplement):S1-04-S01-04.
11. Rugo H*, et al.* (2016) Preliminary efficacy and safety of pembrolizumab (MK-3475) in patients with PD-L1–positive, estrogen receptor-positive (ER+)/HER2-negative advanced breast cancer enrolled in KEYNOTE-028. *Cancer Research* 76(4 Supplement):S5-07-S05-07.

Financial Interests

R.K.J. received an honorarium from Amgen; consultant fees from Enlight, Merck, Ophthotech, Pfizer, SPARC, and SynDevRx; owns equity in Enlight, Ophthotech, and SynDevRx; and serves on the Boards of Trustees of H&Q Healthcare Investors, H&Q Life Sciences Investors, the Tekla Healthcare Opportunities Fund and the Tekla World Healthcare Fund. R.S.L. receives licensing fees (to patents in which he was an inventor on) from, invested in, consults (or was on scientific advisory boards or boards of directors) for, lectured (and received a fee), or conducts sponsored research at MIT for which he was not paid for the following entities – 480 Medical, 7th Sense, Abpro, Aleph Farms, Alkermes, Allevi, Alnylam, Artificial Cells, Arsenal Medical, BASF, Celero, Cellomics, Cellular Biomedical, Clarus, Clontech, Conference Forum, Curis, Domain, Eagle, Echo, Edge, Editas, Evox, Fate Therapeutics, Frequency Therapeutics, Gecko, Genscript, Glycobia, Glympse, Grandhope, Greenlight, HKF Technologies, Horizon Discovery, Humacyte, Indivor, Inovio, Institute of Immunology, In Vivo Therapeutics, Ironwood Pharmaceuticals, Kala, Kallyope, Kensa, Keratinx, KSQ Therapeutics, Landsdowne Labs, Like Minds, Luminopia, Luye, Lyndra, Medical Kinetics, Merck, Micelle, Moderna, Momenta, Monsanto, Mylan, Nanobiosym, Nanobiotix, Noveome, Perosphere, Pfizer, Polaris, Portal, Pulmatrix, Puretech, Roche,Rubius, Secant, Selecta Biosciences, Setsuro, Shiseido, Sigilon, Sio2, SQZ, Stembiosys, Suono Bio, T2 Biosystems, Tara, Taris Biomedical, Tarveda, Third Rock, Tiba, Titan Pharma, Unilever, Vivitex, Wiki Foods, and Zenomics.